

RESEARCH ARTICLE | Control of Movement

Dynamics of human subthalamic neuron phase-locking to motor and sensory cortical oscillations during movement

Witold J. Lipski,^{1,3} Thomas A. Wozny,¹ Ahmad Alhourani,¹ Efstatios D. Kondylis,¹ Robert S. Turner,^{2,3,4} Donald J. Crammond,¹ and Robert Mark Richardson^{1,2,3,4}

¹Brain Modulation Laboratory, Department of Neurological Surgery, University of Pittsburgh School of Medicine, Pittsburgh, Pennsylvania; ²Department of Neurobiology, University of Pittsburgh School of Medicine, Pittsburgh, Pennsylvania; ³Center for the Neural Basis of Cognition, University of Pittsburgh, Pittsburgh, Pennsylvania; and ⁴University of Pittsburgh Brain Institute, Pittsburgh, Pennsylvania

Submitted 23 December 2016; accepted in final form 1 June 2017

Lipski WJ, Wozny TA, Alhourani A, Kondylis ED, Turner RS, Crammond DJ, Richardson RM. Dynamics of human subthalamic neuron phase-locking to motor and sensory cortical oscillations during movement. *J Neurophysiol* 118: 1472–1487, 2017. First published June 7, 2017; doi:10.1152/jn.00964.2016.—Coupled oscillatory activity recorded between sensorimotor regions of the basal ganglia-thalamocortical loop is thought to reflect information transfer relevant to movement. A neuronal firing-rate model of basal ganglia-thalamocortical circuitry, however, has dominated thinking about basal ganglia function for the past three decades, without knowledge of the relationship between basal ganglia single neuron firing and cortical population activity during movement itself. We recorded activity from 34 subthalamic nucleus (STN) neurons, simultaneously with cortical local field potentials and motor output, in 11 subjects with Parkinson's disease (PD) undergoing awake deep brain stimulator lead placement. STN firing demonstrated phase synchronization to both low- and high-beta-frequency cortical oscillations, and to the amplitude envelope of gamma oscillations, in motor cortex. We found that during movement, the magnitude of this synchronization was dynamically modulated in a phase-frequency-specific manner. Importantly, we found that phase synchronization was not correlated with changes in neuronal firing rate. Furthermore, we found that these relationships were not exclusive to motor cortex, because STN firing also demonstrated phase synchronization to both premotor and sensory cortex. The data indicate that models of basal ganglia function ultimately will need to account for the activity of populations of STN neurons that are bound in distinct functional networks with both motor and sensory cortices and code for movement parameters independent of changes in firing rate.

NEW & NOTEWORTHY Current models of basal ganglia-thalamocortical networks do not adequately explain simple motor functions, let alone dysfunction in movement disorders. Our findings provide data that inform models of human basal ganglia function by demonstrating how movement is encoded by networks of subthalamic nucleus (STN) neurons via dynamic phase synchronization with cortex. The data also demonstrate, for the first time in humans, a mechanism through which the premotor and sensory cortices are functionally connected to the STN.

Parkinson's disease; subthalamic nucleus; spike phase-locking; basal ganglia; beta oscillations; deep brain stimulation; motor cortex

STANDARD NEURONAL FIRING RATE-based models of basal ganglia function do not adequately explain many aspects of basal ganglia organization, such as the contributions of first-order, “hyperdirect” projections of cortical neurons to the subthalamic nucleus (STN) or the mechanisms through which the integration of sensory information occurs in the circuit. In addition to afferents from the external globus pallidus, the primate STN receives direct projections from broadly distributed cortical areas including primary motor cortex, premotor cortex, supplementary motor area, dorsolateral prefrontal, anterior cingulate, and inferior frontal cortex (Afsharpoor 1985; Haynes and Haber 2013; Nambu et al. 1997; Parent and Hazrati 1995). In rodents, the STN additionally has been reported to receive direct inputs from primary somatosensory cortical areas (Canteras et al. 1990). Microelectrode recording (MER) in subjects with Parkinson's disease (PD) and in non-human primates has shown that many neurons in the sensorimotor STN modulate their spiking activity during active movement and in response to proprioceptive stimulation (Abosch et al. 2002; DeLong et al. 1985; Georgopoulos et al. 1983; Rodriguez-Oroz et al. 2001; Romanelli et al. 2004; Schrock et al. 2009; Starr et al. 2003; Theodosopoulos et al. 2003; Wichmann et al. 1994). Additionally, the STN has been the subject of numerous local field potential (LFP) recording-based studies in PD patients undergoing deep brain stimulation (DBS) surgery, resulting in a proposed role for the STN in motor response inhibition during decision making. For example, single-unit firing rates and rhythms, as well as low-frequency cortico-subthalamic LFP oscillations, have been suggested to track with the difficulty level of a choice (Alegre et al. 2013; Zaghloul et al. 2012; Zavala et al. 2014, 2016, 2017); however, other known cortical inhibitory processes that contribute to movement selection are thought to begin too early to be mediated by output from the basal ganglia (Turner and Desmurget 2010). Thus STN function is likely complex and not adequately described by binary changes in firing rates.

Address for reprint requests and other correspondence: R. M. Richardson, Dept. of Neurological Surgery, University of Pittsburgh Medical Center, 200 Lothrop St., Suite B400, Pittsburgh, PA 15217 (e-mail: richardsonrm@upmc.edu).

Wichmann et al. (1994) found that a majority of single neurons in the STN increase their firing rate beginning around the time of movement onset but after the onset of muscle activity, suggesting that the sensorimotor territory of the STN participates in the modulation of ongoing movement. Changes in firing rate alone, however, cannot fully account for functional effects observed after clinical and experimental insults to basal ganglia nuclei (DeLong and Wichmann 2007; Nambu et al. 1997); furthermore, evidence of oscillatory activity in STN neurons (Bevan et al. 2002; Gale et al. 2009) suggests that firing pattern may participate in information transfer within the circuit. Indeed, PD has been associated with both abnormal synchronization of activity in the STN within the beta (12–35 Hz) frequency band (Brown 2003; Hammond et al. 2007; Kühn et al. 2009) and rhythmic STN neuronal discharge at oscillations in the beta range at rest (Schrock et al. 2009; Steigerwald et al. 2008; Yang et al. 2014). One physiological mechanism for the modulation of firing pattern is synchronization with specific frequencies in the LFP, where the probability of spiking is modulated by the phase of LFP oscillations. In PD subjects undergoing DBS surgery, simultaneous LFP and MER recordings within the STN have been used to explore the resting spatiotemporal relation of spiking to nested LFP oscillations (Yang et al. 2014). Furthermore, Shimamoto et al. (2013) described a relationship of STN spiking to LFP sampled from the primary motor cortex of PD subjects at rest. Two distinct types of STN spike-to-M1 LFP phase-locking were described: 1) spike locking to the phase of low-frequency oscillations (theta-beta range; 4–30 Hz), and 2) spike locking to the amplitude envelope of high-frequency oscillations (gamma band; 50–200 Hz). Together, these results suggest that STN spikes are locked to the phase of phase-amplitude-coupled oscillations in cortex.

The influence of motor behavior on spike-field relationships is not known; however, we recently demonstrated that excessive phase-amplitude coupling (PAC) in sensorimotor cortex is reduced dramatically during movement in subjects with PD and essential tremor (Kondylis et al. 2016). In the current study, we tested whether STN spike phase-locking is also modulated dynamically during movement by examining the synchronization of neuronal firing in the STN with oscillatory activity in sensorimotor cortex during a bimanual grip force reaction time task.

MATERIALS AND METHODS

Subjects and surgery. Subjects were movement disorders patients undergoing awake DBS surgery for PD. Unified Parkinson's disease rating scale (UPDRS) testing was administered by a neurologist within 4 mo before DBS surgery. Subjects were designated as tremor dominant if the ratio of their mean tremor subscores (UPDRS 3.20, 3.21) to the mean of their gait and postural stability subscores (UPDRS 3.29, 3.30) exceeded 1.5 (Stebbins et al. 2013). All subjects underwent overnight withdrawal from or a reduced dose of their dopaminergic medication before surgery. Targeting and MER were performed using standard clinical techniques for STN DBS (Starr et al. 2003). All participants provided written, informed consent in accordance with a protocol approved by the Institutional Review Board of the University of Pittsburgh (IRB Protocol no. PRO13110420).

Recording. Unit recordings were carried out using single glass-insulated platinum-iridium microelectrodes (FHC, Bowdoin ME) with

impedances between 0.5 and 1.0 MΩ. Signals were filtered and amplified using the Guideline 4000 LP+ system (FHC; 125 Hz–20 kHz), digitized at 30 kHz using the Grapevine Neural Interface System (NIPS; Ripple, Salt Lake City, UT), and saved to a computer for analysis. In one subject, the recordings were carried out using the Neuro-Omega recording system (Alpha Omega, Alpharetta, GA) using Parylene-insulated tungsten microelectrodes. Electrocorticography (ECOG) data were recorded using a strip electrode placed temporarily in the subdural space through the burr hole, with either a 1 × 4, 1 × 6, or 1 × 8 ($n = 10$; 2.3-mm exposed electrode diameter, 10-mm interelectrode distance) or a 2 × 14 [$n = 1$; 1.2-mm exposed electrode diameter, 4-mm interelectrode distance; high-density (HD) contacts] contact platinum-iridium cortical strip electrodes (Ad-Tech Medical Instrument). ECOG signals were online notch filtered at 60, 120, and 180 Hz, bandpass filtered (0.3–250 Hz), amplified, and digitized at 1,000 Hz using the Grapevine NIPS.

Grip task. The behavioral paradigm, a visually cued, instructed delay handgrip task with monetary incentive, was previously described (Kondylis et al. 2016). A single trial of the task began with illumination of the yellow light on a traffic light in the center of the screen and an instructional cue on one side of the screen designating with which hand the subject should subsequently respond by squeezing the handgrip. The instructional cue and yellow light remained illuminated for 1,000–2,000 ms (uniform random distribution), after which the yellow light was extinguished and either the green light (Go cue) or red light (No-Go cue) was illuminated. Following a Go cue, subjects successfully completed the trial if they responded by squeezing a grip force lever (MIE Medical Research, Leeds, UK) with the correct hand in ≤2 s and maintained at least 10% of their previously measured maximum voluntary grip force for ≥100 ms. A trial was counted as an error if subjects did not meet these criteria or inappropriately squeezed during a No-Go trial. Following completion of each trial, a feedback message cued the subject to stop squeezing the handgrip and indicated the winnings or losses for the trial as well as a running balance of winnings. Each trial was followed by a variable intertrial interval (ITI) of 500–1,000 ms. All subjects ($n = 11$) achieved a proficiency of at least 75% correct trials during a preoperative practice period and completed at least 15 successful trials for each hand.

Anatomical localization of ECOG recordings. ECOG recording electrode strip placements were localized on the brain surface by merging an intraoperative fluoroscopy image with a preoperative CT scan and postoperative MRI (Randazzo et al. 2016). The electrodes were categorized according to their anatomical location using automated segmentation in FreeSurfer (Dale et al. 1999; Desikan et al. 2006) as parietal (inferior parietal, superior parietal, supramarginal), postcentral (postcentral gyrus), precentral (precentral gyrus), and frontal (caudal middle frontal, superior frontal).

Unit analysis. MER data were imported into off-line spike-sorting software (Plexon, Dallas, TX) for discrimination of single populations of action potentials using principal components analysis. Spikes were sorted into single units according to standard criteria, including stability of waveforms throughout the recording, presence of a refractory period in the interspike interval distribution of at least 3 ms, and absence of strong modulation of firing by cardiac rate (Schrock et al. 2009; Starr et al. 2003). Recordings that could not be reliably discriminated into single-unit waveforms and that did not meet the minimum refractory period criterion were designated as multiunit recordings. To further ensure that only stable recordings were analyzed, firing rates of all spike time series were then examined over the course of task performance. For every recording, the mean firing rate over the course of each trial was calculated; a consecutive block of task trials was then selected such that the mean firing rate for each trial within the set was within 2 SD of the overall mean firing rate:

$$\left| \overline{FR}_T - FR_t \right| < 2\sigma_{FR,T},$$

where \overline{FR}_T and $\sigma_{FR,T}$ are the mean and SD of firing rates in a consecutive set of trials T , FR_t is the mean firing rate within trial t , and $t \in T$.

Timestamp data were used to calculate average firing rate histograms with regard to movement onset, using MATLAB software (The MathWorks, Natick, MA). Spiking time series were divided into 5-s epochs aligned on the grip force inflection points of all correct Go trials and then divided into 100-ms bins. Premovement baseline firing was defined using a 1-s ITI epoch preceding cue presentation for each trial; baseline firing distributions for each recording were computed from the aggregate of these within-trial baseline epoch bins. Significant modulation by movement was defined as the occurrence of two consecutive bins outside the 95% confidence interval of the baseline distribution within a window of 200 ms before to 1 s after movement onset.

Unit spectral characteristics. Oscillatory patterns in the spike times were computed between 0 and 50 Hz using the global spike-shuffling method (Rivlin-Etzion et al. 2006; Shimamoto et al. 2013). The power spectral density (PSD) was estimated using MATLAB pwelch function, using a 2-s sliding window with 50% overlap, resulting in a frequency resolution of 0.5 Hz. Spectra were normalized to those obtained by randomly shuffling spike times 100 times; and the significance threshold was set at 2 SD above the mean of the 300- to 500-Hz part of the normalized spectrum (Rivlin-Etzion et al. 2006).

Spectral analysis. To quantify the changes in oscillatory power within each frequency band of interest, activation weights (AW) for 1-s pre- and postmovement epochs of ECoG were calculated, using a 1-s pre-Cue time segment (ITI) as baseline (Miller et al. 2007):

$$AW_{M,ITI} = \frac{(\overline{M} - \overline{ITI})^3}{\left| \overline{M} - \overline{ITI} \right| \sigma_{M \cup ITI}^2} \frac{N_M N_{ITI}}{N_{M \cup ITI}^2}$$

M and ITI signify the trialwise distribution of band power within the movement and ITI epochs, respectively; N represents the number of trials, and σ and an overbar denote the SD and mean, respectively. AWs are signed squared cross-correlation values reflecting the degree to which the variance in power across movement and ITI epochs is explained by the corresponding difference in the mean power (Miller et al. 2007). PSD was calculated using the MATLAB pwelch function, using a 256-point (256 ms) sliding window with 50% overlap.

High-frequency activation. The presence of high-frequency activation (HFA) by contralateral grip squeeze was tested in each ECoG electrode contact for each subject. First, the signal was bandpass filtered (75–200 Hz; EEGLAB function eegfilt; Delorme and Makeig 2004), and the Hilbert amplitude was applied to the resulting broadband gamma signal. The gamma amplitude was then averaged within five nonoverlapping 1-s epochs centered on contralateral movement onset for each trial. Similarly, the baseline broadband gamma amplitude was computed for the 1-s ITI epoch for each trial. The change from baseline broadband gamma power was then expressed for each of the five time epochs as a trialwise t statistic. HFA contacts were defined as those that had a t statistic corresponding to a P value of 0.01 (5% confidence interval corrected for 5 observations) in at least one of five time epochs. In those subjects where more than one HFA contact was identified, the contact with the highest broadband gamma t statistic is reported.

Spike phase-locking. Two types of coherence between STN spike times and LFPs were examined: beta spike phase-locking (β -SPL) and gamma amplitude envelope spike phase-locking (γ AE-SPL). For β -SPL analysis, the spectral content of common average referenced LFPs recorded at subdural electrodes was estimated using complex-valued Morlet wavelets (4–40 Hz). For γ AE-SPL analysis, common average referenced LFPs were first bandpass filtered between 75 and 200 Hz (MATLAB eegfilt function), and the amplitude of the Hilbert transform was computed on the resulting broadband gamma signal. The resultant complex values were normalized to have unit length. For each subdural electrode, spike timestamps from each concurrently recorded STN unit were used to epoch and align LFP spectral estimates from 500 ms before to 500 ms after spike firing. Complex values were then averaged across spike-triggered epochs within each time-frequency point, and absolute value of the modulus was taken to represent the strength of spike-field coherence (phase-locking factor, PLF). To normalize these values to the phase-locking expected by chance given each LFP and spike time series, a null PLF distribution was generated. One hundred surrogate PLF time-frequency matrices were calculated using an LFP time series circularly shifted by a random time lag (MATLAB rand function). z -PLF values at each time-frequency point were then calculated on the basis of the mean and SD of the surrogate distribution; z values were calculated as a function of phase frequency (4–40 Hz) and lag time relative to spike (± 500 ms) for each unit recording and cortical contact within every subject. Significant z -PLF clusters within each condition were then

Table 1. Clinical characteristics of study subjects

Subject	Age, yr	Sex	MMSE Score	Tremor Dominant	UPDRS Motor Subscores in OFF-Medication State												Total UPDRS III	
					Rest Tremor Amplitude		Postural Tremor of the Hands		Finger Tapping		Hand Movement		RAM					
					R	L	R	L	R	L	R	L	R	L	R	L		
1	69	F	29/30	No	0	2	0	0	1	1	1	1	1	1	1	1	31	
2	54	F	29/30	NR	NR	NR	NR	NR	NR	NR	NR	NR	NR	NR	NR	NR	NR	
3	68	M	29/30	No	0	1	0	1	2	3	2	3	1	3	1	3	42	
4	66	M	30/30	Yes	3	3	2	3	3	3	3	3	3	2	3	2	62	
5	71	M	30/30	No	2	0	0	0	3	2	3	3	3	3	3	3	55	
6	65	F	26/30	No	0	1	1	1	2	4	2	3	2	2	2	2	54	
7	45	M	29/30	Yes	3	3	4	4	0	1	0	1	0	1	0	1	31	
8	60	M	29/30	No	2	3	1	1	2	3	2	2	2	2	2	2	52	
9	54	M	30/30	No	1	0	0	0	2	2	2	2	3	3	3	3	33	
10	68	M	NR	No	0	0	2	2	2	3	2	2	2	3	2	3	48	
11	52	M	NR	No	0	0	0	0	1	1	1	1	1	1	1	1	27	

Summary of the demographic description of the subject cohort, including neurocognitive assessment and symptom severity. M/F, male/female; MMSE, Mini Mental State Exam for neurocognition; UPDRS, Unified Parkinson's Disease Rating Scale; RAM, rapid alternating movements of the hands; NR, value was not recorded in the medical record.

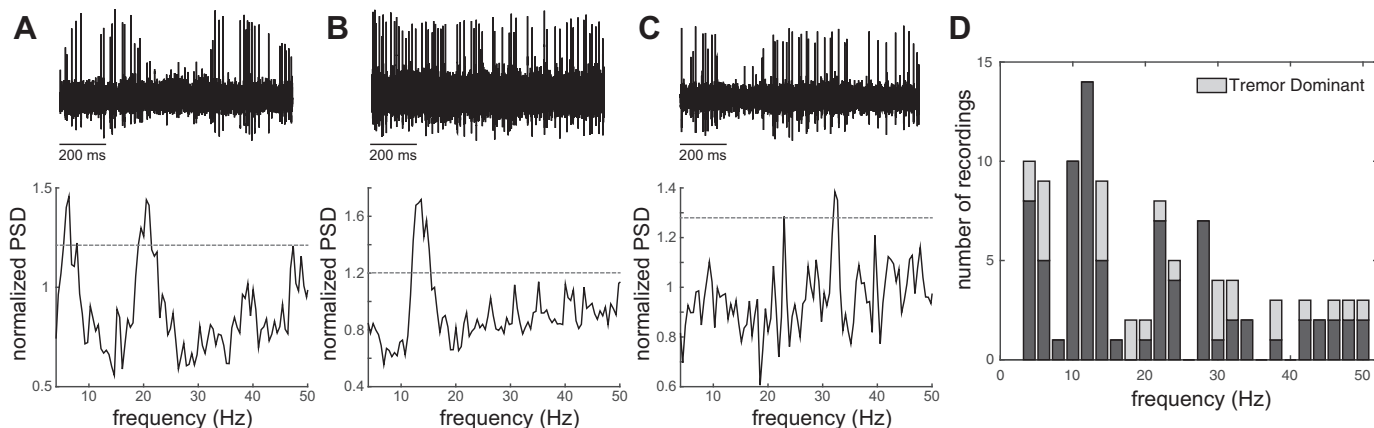


Fig. 1. Examples of voltage traces and power spectra of STN recordings from a single unit with theta and beta (A), a multiunit with low-beta (B), and a single unit with high-beta oscillatory frequencies (C; significance threshold is indicated by dashed line in each plot). D: distribution of significant frequency components in neuronal spike recordings in the STN. Unit oscillatory frequency did not appear to depend on the subject's tremor dominant symptom category. PSD, power spectral density.

identified by thresholding using a cluster-based nonparametric permutation method (Maris and Oostenveld 2007). Cluster thresholding was performed within the beta frequency band (12–40 Hz). This was done because the *z*-PLF cluster thresholding algorithm takes into account cluster size and therefore has a slight inherent bias toward clusters at lower frequencies. Thus confining the analysis to within the frequency band of interest resulted in a more accurate representation of significant SPL. Movement-related spike phase-locking was characterized within 26 one-second sliding windows time-shifted by 200 ms and centered on ipsilateral and contralateral movement onset.

Clustering of significant SPL. Significant spike-field locking was defined using cluster-based nonparametric permutation testing (Maris and Oostenveld 2007). Each *z*-PLF time-frequency plot was thresholded to a *z*-score value equivalent to $P < 0.05$. Contiguous suprathreshold pixels were grouped into clusters using MATLAB's image processing toolbox, and the sum of the *z* scores within each cluster was calculated. The same procedure was applied to the time-frequency *z*-PLF plots of the previously generated random surrogates, however, only the largest cluster sum was retained in each permutation to build a distribution of cluster significance. A *P* value was assigned to the clusters in the real *z*-PLF plots on the basis of the probability of finding a similar cluster *z*-score sum value in the surrogate distribution. Each significant *z*-PLF cluster was characterized on the basis of its peak (maximum) phase frequency and time lag. Testing for differences in *z*-PLF time-frequency plots between movement epochs and ITI epochs was carried out using a similar permutation method. A paired *t*-statistic describing the group difference between the ITI and each movement epoch *z*-PLF was calculated for each time-frequency point. The same procedure was applied to 1,000 surrogate data sets that were generated by randomly scrambling ITI and movement epoch *z*-PLF plots. The *t*-statistic time-frequency plots were then thresholded to a *z*-score value equivalent to $P < 0.05$, and the significance of resulting clusters was identified as described above. Testing for differences in the *z*-PLF time-frequency plots between contralateral and ipsilateral movement epochs was carried out in the same manner. To summarize movement-related changes in phase-locking, total positive (increase) and negative (decrease) cluster *t*-statistics are reported, along with the cluster range in time-frequency space and total cluster *P* values (Fisher's method for combining *P* values was used when multiple clusters were present within a time epoch).

Correlation of β -SPL with spectral power and firing rate. To test whether movement-related changes in β -SPL might be due to simultaneous modulation of cortical spectral power and STN firing rate, the

change in β -SPL was correlated with corresponding changes in low-beta power, high-beta power, and firing rate at each movement time point relative to the ITI baseline. Changes in β -SPL were computed by taking the mean *z*-PLF value in the range of ± 200 -ms lag times and 12–24 Hz (for correlating with low-beta power), 25–40 Hz (for correlating with high-beta power), and 12–40 Hz (for correlating with firing rate) at each movement epoch for each unit-contact pair and subtracting the respective mean *z*-PLF during the ITI baseline. Corresponding changes in power were computed as activation weights (AWs; see *Spectral analysis* above). Firing rate changes were computed as the fractional change in firing rate for each movement epoch relative to the ITI baseline: Δ firing rate(*t*) = [firing rate(*t*) – firing rate_{ITI}]/firing rate_{ITI}. Linear

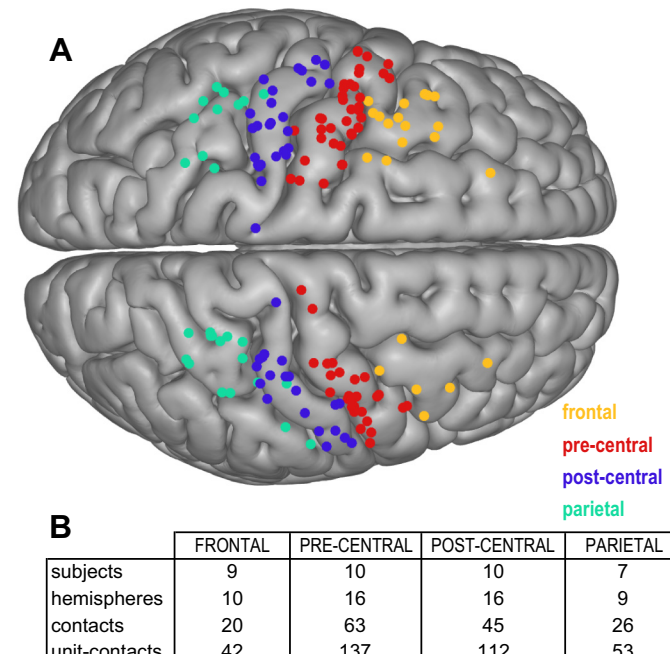


Fig. 2. Anatomic categorization of ECoG recordings. A: ECoG electrode contact locations were categorized into parietal (inferior parietal, superior parietal, supramarginal), postcentral (postcentral gyrus), precentral (precentral gyrus), and frontal (caudal middle frontal, superior frontal) anatomical regions based on the Desikan-Killiany labeling system. B: chart showing the number of subjects, hemispheres, contacts, and unit-contact pairs recorded within each anatomical region.

regression was performed (MATLAB regress function), and both linear (Pearson) and rank-order (Spearman) regression coefficients were calculated (MATLAB corr function).

RESULTS

Grip task performance. Eleven PD subjects performed a visually cued, bimanual grip force task. Table 1 summarizes the demographic description of the subject cohort. Two of 11 subjects were categorized as tremor dominant. The mean grip reaction time (RT) to the Go stimulus was 0.45 ± 0.04 s (left) and 0.49 ± 0.05 s (right). The mean maximum grip force (F_{\max}) produced was 92.8 ± 16.7 N (left) and 115.4 ± 22.2 N (right). A subset of these subjects (5 of 11) constituted part of a previously published cohort of PD patients (Kondylis et al. 2016). As reported there, kinematics during task performance did not differ from those of subjects without a movement disorder (Kondylis et al. 2016), demonstrating that PD patients were able to perform the motor task.

Neuronal spike recordings. Thirty-four STN unit recordings were completed during task performance (mean firing rate 28.1 ± 2.3 Hz). Of these recordings, 18 were categorized as representing single neurons and 16 were categorized as multi-unit, based on the interspike interval distribution and waveform principal component analysis. In three cases, two distinct single units were discriminated from a single recording. Fourier analysis revealed oscillatory firing patterns with significant frequency components in the theta and alpha bands (4–11 Hz; $n = 14$), low-beta range (12–24 Hz; $n = 12$), and high-beta range (25–40; $n = 8$). Twelve units exhibited oscillatory

patterns within multiple bands. Figure 1 shows examples of recorded voltage traces and power spectra of three STN units. Unit oscillatory frequency did not appear to depend on the subject's tremor dominant symptom category.

Anatomical locations of ECoG recording contacts. The locations of ECoG recording contacts were mapped to one of four cortical regions: frontal ($n = 20$; 0 HD), precentral ($n = 63$; 12 HD), postcentral ($n = 45$; 14 HD), and parietal ($n = 26$; 2 HD) (Fig. 2). The number of subjects and hemispheres with coverage of these cortical areas, as well as the total number of unit-contact pairs (the product of the number of individual STN units and concurrently recorded ECoG contacts), is indicated in Fig. 2B.

Spectral characteristics of cortical LFP recordings. Oscillatory LFP activity within the low-beta band (12–24 Hz), high-beta band (25–40 Hz), and broadband gamma band (50–200 Hz) in each cortical region was examined during a 5-s time window surrounding grip force onset. Oscillatory power, quantified as AWs for each frequency band, was calculated relative to the ITI baseline and characterized for each region during grip responses ipsilateral and contralateral to the recorded hemisphere (Fig. 3). Grip movements on both ipsilateral and contralateral sides were associated with suppression of beta power in all regions, which was more pronounced for movements with the contralateral hand than with the ipsilateral hand (Fig. 3, A and B; $P < 0.05$, sign test, Bonferroni corrected for multiple comparisons). Gamma synchronization was increased selectively during contralateral grip, within pre- and postcentral regions (Fig. 3C; $P < 0.05$, sign test, Bonferroni corrected for multiple comparisons).

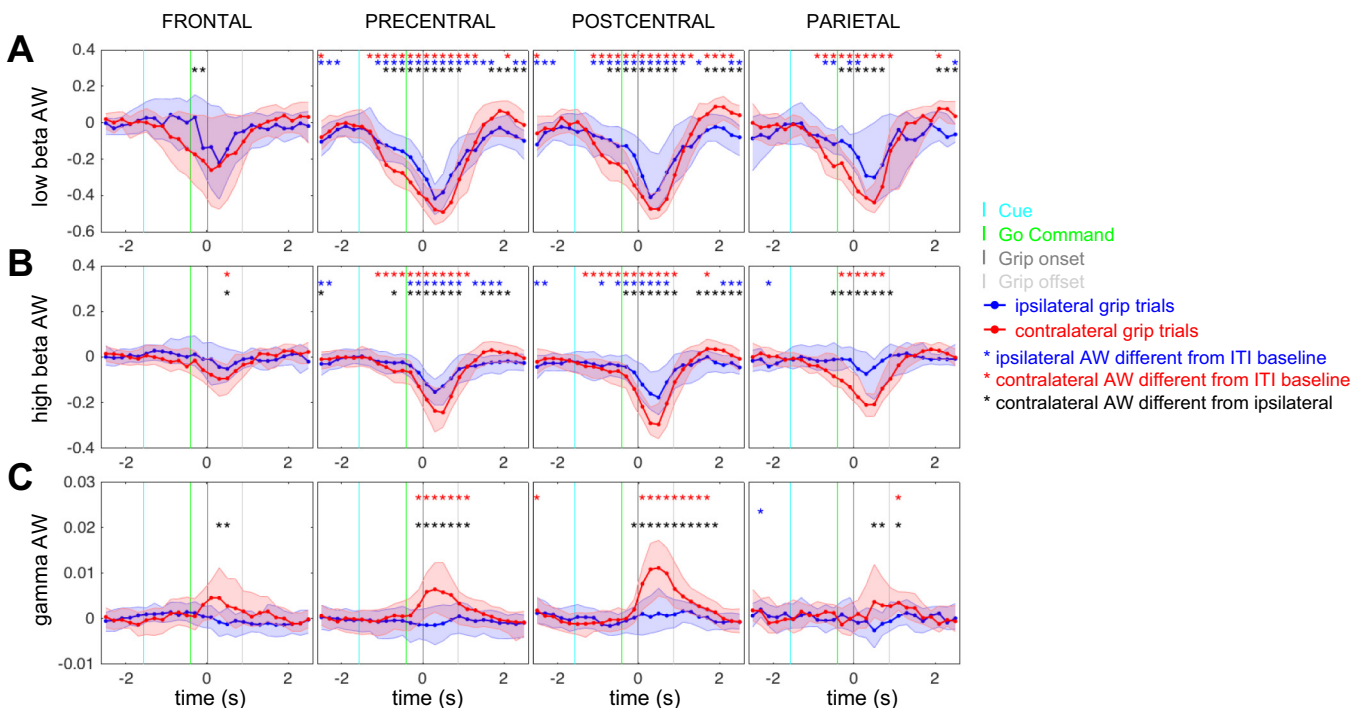


Fig. 3. Cortical spectral power changes during movement. Application of grip force with the hand contralateral to the recording hemisphere was associated with a suppression of oscillatory power in the low-beta (A; 12–24 Hz) and high-beta range (B; 25–40 Hz) and an increase in power in the broadband gamma range (C; 75–200 Hz). A similar pattern was observed in frontal, precentral, postcentral, and parietal recording sites. Application of grip force with the hand ipsilateral to the recording hemisphere also resulted in beta power suppression; however, it did not elicit a broadband gamma response. Red asterisks denote time points at which activation weights (AW) during contralateral grips are significantly different from zero (different from ITI baseline). Blue asterisks denote time points at which AWs during ipsilateral grips are significantly different from zero. Black asterisks denote time points at which AWs during contralateral grips are significantly different from ipsilateral grips (sign test, Bonferroni corrected for multiple comparisons, $P < 0.05$).

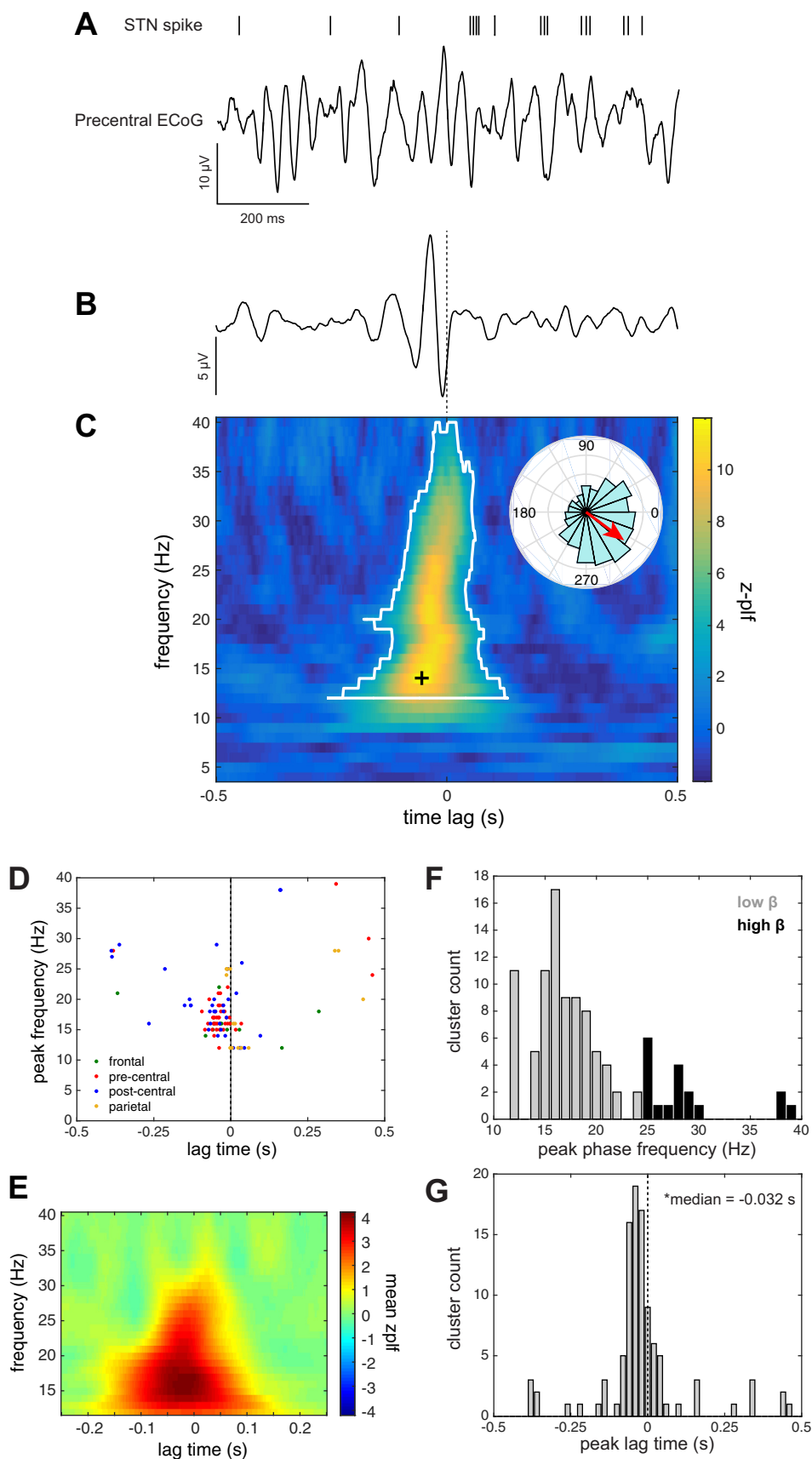
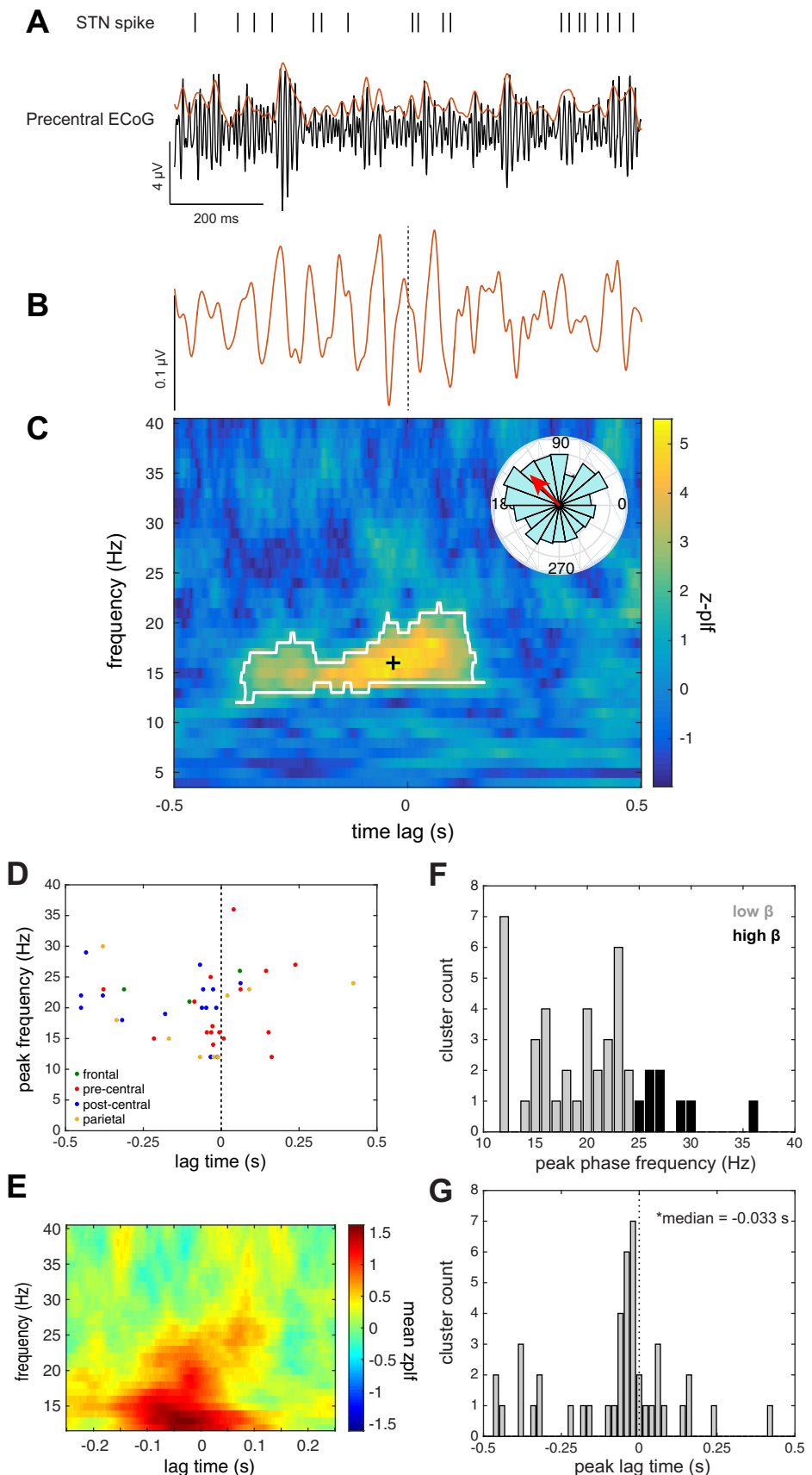


Fig. 4. STN beta spike phase-locking (β -SPL) during ITI. *A*: example of simultaneous STN neuronal spike times shown relative to an ECoG signal from an electrode contact localized to the precentral gyrus during a single 1-s, movement-free ITI baseline epoch. *B*: spike-triggered average (STA) of the ECoG signal shown in *A*, based on 660 STN spikes fired over the course of 44 ITI epochs, showing a brief oscillation preceding the spike time (dashed line). *C*: this relationship was quantified as a z -scored phase-locking value as a function of phase frequency and lag time relative to spike. To identify phase-locking significantly different from that expected by chance, a β -SPL cluster (white outline) within this time-frequency space was computed using a cluster-based nonparametric permutation method. Note that the clustering was done within the beta frequency range (12–40 Hz) only, effectively setting bounds on cluster frequencies. Each cluster was characterized by its peak z -PLF time-frequency point (black cross). *Inset* polar plot in *C* shows the distribution of phase angles at the indicated peak z -PLF time-frequency point and its mean phase angle (red arrow). *D*: group data showing the distribution of the peak frequencies and lag times of β -SPL clusters within each anatomical region. *E*: β -SPL represented as mean z -PLF values across all unit-contact pairs. *F*: histogram of peak β -SPL cluster frequencies. *G*: histogram of peak cluster lag times. Lag times were distributed around a median of -32 ms (1st quartile = -55 ms, third quartile = 5 ms), which was significantly less than zero (sign test, $P < 10^{-5}$).



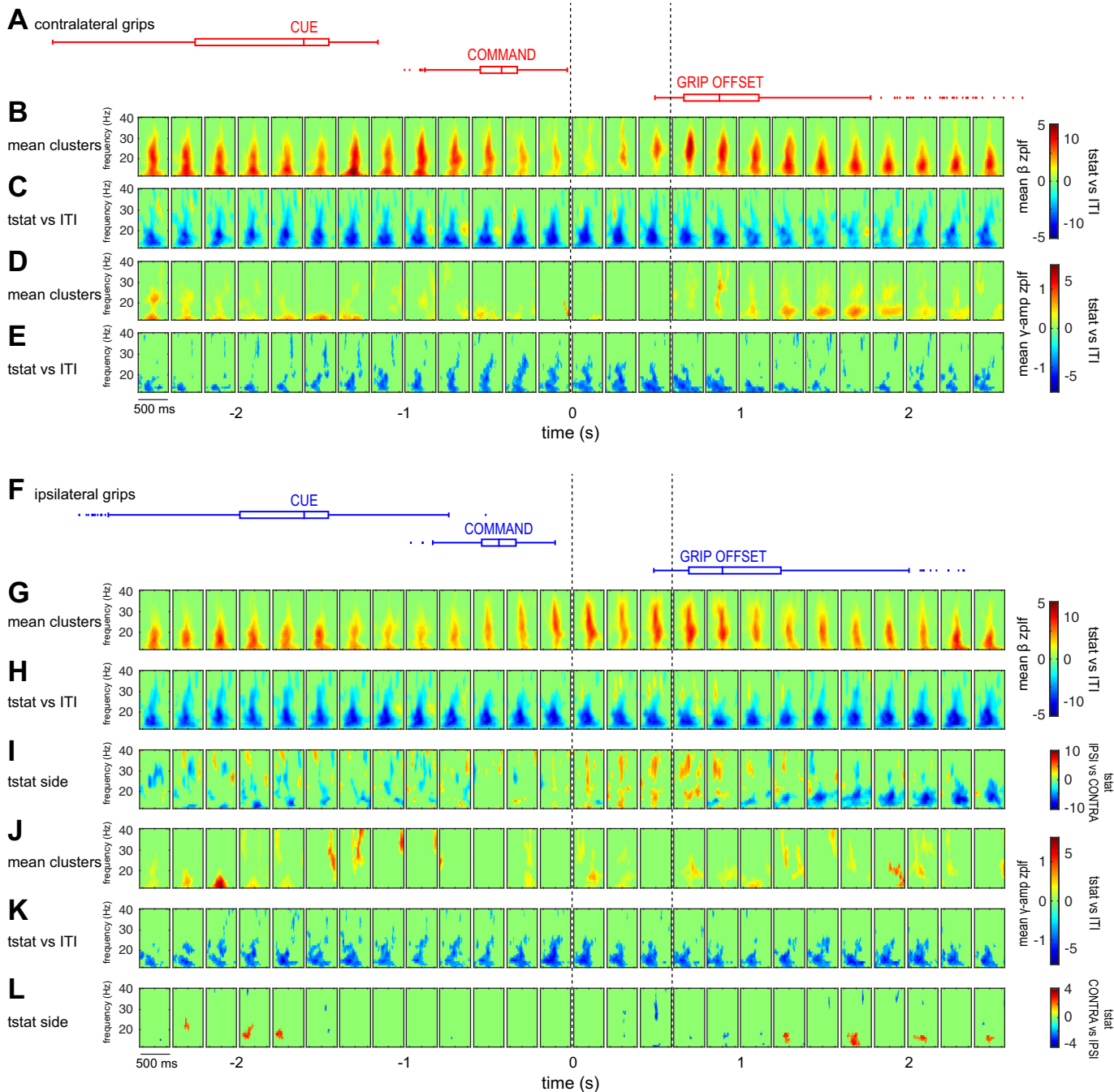


Fig. 6. Contralateral and ipsilateral grip force application is associated with a suppression of β -SPL and γ AE-SPL, and selective increases in β -SPL: group summary of STN spike phase-locking across movement time course. *A*: box plots indicating cue, command, and feedback stimulus times, as well as grip offset times, for all contralateral grip trials. *B*: mean β -SPL z -PLF cluster values shown at each time point relative to contralateral grip force onset. *C*: clusters of t -statistics (t stat) showing significant change in β -SPL from the ITI for contralateral grip trials. *D*: mean γ AE-SPL z -PLF cluster values shown at each time point for contralateral grip trials. *E*: clusters of t -statistics showing significant change in γ AE-SPL from the ITI for contralateral grip trials. *F*: box plots indicating cue, command, and feedback stimulus times, as well as grip offset times, for all ipsilateral grip trials. *G*: mean β -SPL z -PLF cluster values shown at each time point relative to ipsilateral grip force onset. *H*: clusters of t -statistics showing significant change in β -SPL from the ITI for ipsilateral grip trials. *I*: clusters of t -statistics showing significant difference in β -SPL between contralateral and ipsilateral grips (positive t stat values indicate greater β -SPL for contralateral grips). *J*: mean γ AE-SPL z -PLF cluster values shown at each time point, for ipsilateral grip trials. *K*: clusters of t -statistics showing significant change in γ AE-SPL from the ITI for ipsilateral grip trials. *L*: clusters of t -statistics showing significant difference in γ AE-SPL between contralateral and ipsilateral grips (positive t stat values indicate greater γ AE-SPL for contralateral grips). Clusters of t -statistics are computed using paired permutation testing ($P < 0.05$). Note that the mean significant cluster plots (*B*, *D*, *G*, *J*) depict only the mean of z -PLF cluster values for neuron-contact pairs that showed significant SPL at a given time point; t -statistic plots (*C*, *E*, *H*, *I*, *K*, *L*) reflect the comparison of z -PLF values for all neuron-contact pairs, regardless of the presence of significant z -PLF clusters. All data are aligned to grip onset ($t = 0$). Dotted lines outline the 3 time points within 500 ms following movement onset for which t -statistics are listed in Table 4.

STN neuron firing is phase-locked to LFPs in broadly distributed cortical areas during the ITI. The ITI task epoch was used to examine synchronization of STN firing to the phase of cortical LFP oscillations during periods without movement (ITI). β -SPL in the precentral gyrus was observed in 10 units (5/10 subjects; 39/137 unit-contact pairs), confirming the findings of Shimamoto et al. (2013). An example of a neuron synchronized to motor cortex beta oscillations is shown in Fig. 4A. Phase-locking during the ITI was not specific to oscillations in the precentral cortex but also was observed for frontal (8 units; 6/9 subjects; 12/42 unit-contact pairs), postcentral (10 units; 4/10 subjects; 35/112 unit-contact pairs), and parietal (4 units; 3/7 subjects; 15/53 unit-contact pairs) regions (Fig. 4, D–F). Lag times across all the cortical regions were

significantly different from zero [median = −32 ms, interquartile range (IQR) = (−55 5) ms; $P < 10^{-5}$, sign test], indicating that the consistent cortical phase appeared before STN spike firing (Fig. 4G). Peak frequencies and lag times were not significantly different between cortical regions (Kruskal-Wallis test; lag times $P = 0.35$; frequencies $P = 0.47$).

Gamma amplitude spike phase-locking during the ITI. Similarly, synchronization with the phase of oscillations in the cortical gamma (75–200 Hz) amplitude envelope (γ AE-SPL) was also examined during the ITI. Figure 5A shows an example of STN activity that is synchronized to the gamma amplitude envelope of oscillations in motor cortex. γ AE-SPL was observed to oscillations in precentral gyrus in 10 units (5/10 subjects; 16/137 unit-contact pairs), in agreement with previ-

Table 2. Modulation of β -SPL across regions during 500 ms following movement onset

Decreases in β -SPL Relative to ITI											
Ipsilateral grip t cluster characteristics						Contralateral grip t cluster characteristics					
Time, s	Σt	P value	Frequency range, Hz	Lag range, ms		Time, s	Σt	P value	Frequency range, Hz	Lag range, ms	
<i>Frontal</i>											
0.1	−1.5E+03	0	13	20	−159	95	0.1	−3.2E+03	0	12	29
0.3	−1.1E+03	0	13	36	−145	213	0.3	−3.6E+03	0	13	29
0.5	−1.4E+03	0	13	35	−195	199	0.5	−3.2E+03	0	13	34
<i>Precentral</i>											
0.1	−1.1E+04	0	12	28	−223	201	0.1	−1.0E+04	0	12	31
0.3	−1.0E+04	0	12	30	−251	237	0.3	−1.1E+04	0	12	34
0.5	−9.3E+03	0	12	25	−251	245	0.5	−1.2E+04	0	12	40
<i>Postcentral</i>											
0.1	−8.8E+03	0	12	40	−251	249	0.1	−1.1E+04	0	12	40
0.3	−9.7E+03	0	12	40	−251	249	0.3	−1.1E+04	0	12	40
0.5	−1.0E+04	0	12	40	−251	249	0.5	−9.8E+03	0	12	40
<i>Parietal</i>											
0.1	−8.9E+03	0	12	40	−229	249	0.1	−7.5E+03	0	12	40
0.3	−9.4E+03	0	12	40	−251	249	0.3	−7.9E+03	0	12	38
0.5	−9.2E+03	0	12	40	−251	249	0.5	−8.7E+03	0	12	40
Increases in β -SPL Relative to ITI											
Ipsilateral grip t cluster characteristics						Contralateral grip t cluster characteristics					
Time, s	Σt	P value	Frequency range, Hz	Lag range, ms		Time, s	Σt	P value	Frequency range, Hz	Lag range, ms	
<i>Frontal</i>											
0.1	0.0E+00	1				0.1	4.5E+02	0.048	28	33	−251
0.3	1.0E+03	0.013	26	40	−125	−53	0.3	6.0E+02	0.027	28	35
0.5	5.1E+02	0.048	26	33	−121	−67	0.5	6.5E+02	0.03	29	36
<i>Precentral</i>											
0.1	0.0E+00	1				0.1	0.0E+00	1			
0.3	0.0E+00	1				0.3	0.0E+00	1			
0.5	0.0E+00	1				0.5	0.0E+00	1			
<i>Postcentral</i>											
0.1	0.0E+00	1				0.1	0.0E+00	1			
0.3	0.0E+00	1				0.3	0.0E+00	1			
0.5	0.0E+00	1				0.5	0.0E+00	1			
<i>Parietal</i>											
0.1	2.1E+03	0.002	27	40	−147	249	0.1	0.0E+00	1		
0.3	1.4E+03	0.005	27	40	−143	−13	0.3	5.0E+02	0.036	26	33
0.5	6.4E+02	0.027	28	40	−137	−99	0.5	0.0E+00	1		

Changes in β -SPL relative to ITI were assessed for each movement time point using cluster-based permutation testing, resulting in time-frequency clusters of t -statistics that indicate significant changes in phase locking at given frequencies and lags. The total cluster t -statistic values (Σt) and corresponding P values, as well as ranges in frequency and lag, are shown for clusters representing decreases and increases in β -SPL at 0.1, 0.3, and 0.5 s after movement onset relative to ITI (these time points are indicated with dotted lines in Fig. 6). These statistics are shown separately for movements made with the ipsilateral and contralateral hand and are segregated by anatomical region.

ously reported γ AE-SPL to this region (Shimamoto et al. 2013). In addition, γ AE-SPL during the ITI was observed to oscillations in the frontal (3 units; 3/9 subjects; 3/42 unit-contact pairs), postcentral (10 units; 4/10 subjects; 16/112 unit-contact pairs), and parietal (6 units; 2/7 subjects; 9/53 unit-contact pairs) regions (Fig. 5, *D–F*). Similar to β -SPL lag times, γ AE-SPL appeared before STN spike firing [median = −33 ms, IQR = (−174 14) ms; $P < 0.004$, sign test; Fig. 5*G*]. Peak frequencies and lag times were not significantly different between regions (Kruskal-Wallis test; lag times $P = 0.28$; frequencies $P = 0.51$). Overall, when all cortical regions were taken into account during the ITI epoch, β -SPL was observed in 8/11 subjects, and γ AE-SPL was observed in 8/11 subjects, whereas both β -SPL and γ AE-SPL were observed in 7/11 subjects. Moreover, in a subset of recordings ($n = 25$), STN firing was phase-locked to both the beta oscillations and the gamma envelope of the LFP in the same cortical contact. In these cases, however, the phase-locking frequencies for β -SPL and γ AE-SPL were not correlated (Spearman $\rho = 0.39$, $P = 0.06$), suggesting that these two forms of phase-locking are functionally distinct.

Contralateral movement modulates phase-locking of STN neurons to cortical beta oscillations. Given that STN SPL to motor cortex may be excessive in PD, we examined whether this synchrony was maintained during movement. Contralateral movement primarily suppressed low-beta SPL to all cortical areas examined. We found that for STN neurons whose firing was phase-locked to cortical beta oscillations during the ITI ($n = 108/377$ unit-contact pairs with significant z -PLF clusters), SPL was suppressed during movement of the contralateral hand (group data for contacts in all 4 anatomical regions is shown in Fig. 6, *B* and *C*); however, there were also sparse increases in phase locking at several movement time points, including 1,000 ms preceding movement to 500 ms after movement onset. Thus, within the same movement epoch, SPL increases and decreases relative to baseline occurred simultaneously in the population of recorded units but were characterized by different lag time-phase frequency clusters. Notably, the decoupling of neuronal firing from beta oscillations began before movement onset, at a time corresponding to cue presentation. The population of STN neurons whose phase-locking to cortical beta oscillations during the ITI did not reach significance ($n = 275/377$ unit-contact pairs without significant z -PLF clusters) also showed a decrease in phase coupling during movement. Suppression relative to ITI baseline during the initial 500 ms after movement onset was significant for contacts from each cortical region when examined separately; however, increases in β -SPL were significant only in frontal and parietal contacts during this time frame (permutation testing, $P < 0.05$; see Table 2).

Contralateral movement suppresses phase-locking of STN neurons to the gamma envelope of cortical oscillations. γ AE-SPL in motor cortex has been described at rest in patients with PD (Shimamoto et al. 2013). We found that for neurons that exhibited γ AE-SPL to beta oscillations during the ITI epoch ($n = 48/377$ unit contact pairs with significant z -PLF clusters), this synchrony was suppressed during contralateral movement (Fig. 6, *D* and *E*). Given that gamma power in all cortical regions examined was increased on the group level during movement with the contralateral hand, we asked whether γ AE-SPL was specifically suppressed in HFA contacts, de-

fined as showing the strongest significant broadband gamma increase during movement (see Table 3). Indeed, in three units whose firing showed significant γ AE-SPL to HFA contacts during the ITI, this synchrony was suppressed during contralateral movement, despite significant increases in cortical broadband gamma power.

Ipsilateral movement modulates β -SPL and γ AE-SPL. STN neuron phase-locking to cortical LFPs was also modulated during movement of the hand ipsilateral to the recorded hemisphere. For neurons whose firing was phase-locked to cortical oscillations during the ITI, both β -SPL and γ AE-SPL were suppressed during ipsilateral movement (Fig. 6, *F–L*); however, there also was a selective increase in β -SPL, in the high-beta range (24–40 Hz), within 1,500 ms following movement onset (Fig. 6*H*). Comparison of SPL between ipsilateral and contralateral movement showed significantly stronger β -SPL, but not γ AE-SPL, during ipsilateral movement in the same time frame (Fig. 6, *I* and *L*).

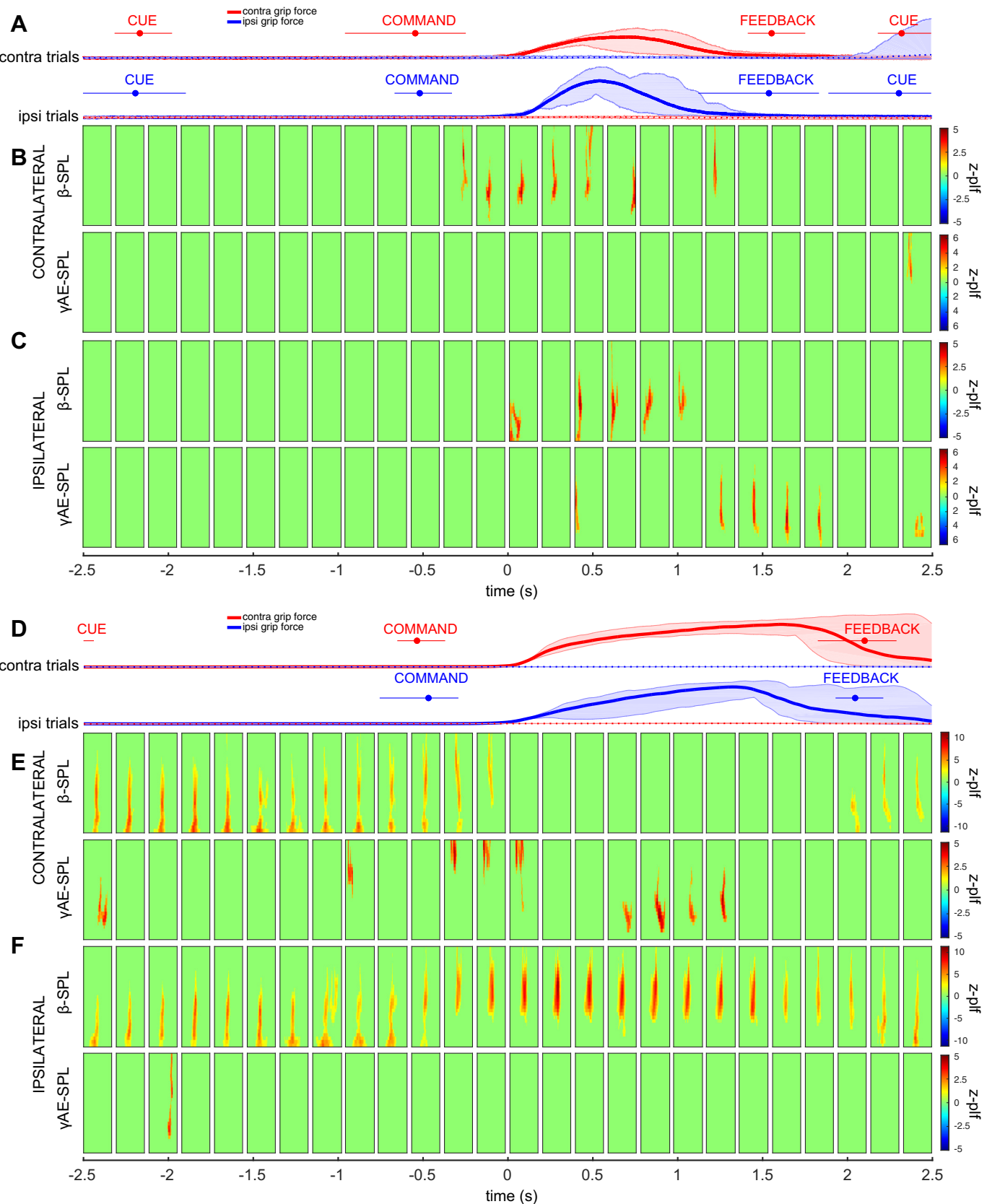
Neurons with increased SPL during movement compared with ITI. Despite a predominant reduction of phase-locking during movement across the population of STN neurons recorded, a proportion of unit-contact pairs exhibited increased phase-locking during movement relative to the ITI epoch or became phase-locked only during movement. Figure 7, *A–C* shows a representative unit recording with β -SPL clusters during ipsilateral grip, along with γ AE-SPL. Figure 7, *D–F* shows a representative unit recording with β -SPL clusters during contralateral grip, along with γ AE-SPL.

Task-related activity of STN neurons does not predict cortical phase synchronization. Sixteen of 35 units exhibited changes in firing rate within the epoch examined around movement onset. Responses to movement were categorized on the basis of modulation of neuronal firing by movement onset during responses ipsilateral and contralateral to the recording site. Selective responses included increased firing following contralateral movement onset ($n = 1$), increased firing following ipsilateral movement onset ($n = 1$), decreased firing following contralateral movement onset ($n = 5$), and decreased

Table 3. HFA contacts

Subject	Side	Region	Peak HFA Epoch, s
1	Left	Precentral	3
1	Right	N/A	N/A
2	Left	Precentral	3
3	Left	Frontal	2
4	Left	Postcentral	3
4	Right	Postcentral	3
5	Left	Precentral	3
5	Right	Parietal	3
6	Left	Postcentral	3
7	Left	Postcentral	3
7	Right	N/A	N/A
8	Left	Postcentral	3
9	Left	Precentral	3
9	Right	Postcentral	3
10	Left	Frontal	3
11	Left	Precentral	3
11	Right	Precentral	3

The presence of high-frequency activation (HFA) ECoG electrode contacts was tested in each hemisphere, in each subject (see METHODS). The anatomical region, as well as the time epoch relative to movement onset, is shown for each HFA contact. N/A indicates that no contact met the criteria for HFA.



firing following ipsilateral movement onset ($n = 1$). Nonselective responses included increased firing following both ipsilateral and contralateral movement onset ($n = 7$) and a complex response involving both inhibition and excitation bilaterally ($n = 1$). Examples are shown in Fig. 8. The neuronal response category was not correlated with anatomic location within the STN or any phase-locking characteristic. No firing rate changes occurred before movement onset.

Movement-related changes in β -SPL are independent of spectral power and firing rate. Given that both ipsilateral and contralateral grips were associated with a broadly distributed suppression of beta power in cortex, we tested whether simultaneously measured suppression in β -SPL was correlated with power changes at the level of individual unit-contact pairs, as well as with spike firing rate. This analysis revealed weak linear and rank order correlations between changes in β -SPL and corresponding changes in low-beta power (ipsilateral movement: Pearson $\rho = 0.02$, Spearman $\rho = 0.09$; contralateral movement: Pearson $\rho = 0.18$, Spearman $\rho = 0.17$), high-beta power (ipsilateral movement: Pearson $\rho = -0.11$, Spearman $\rho = -0.09$; contralateral movement: Pearson $\rho = 0$, Spearman $\rho = -0.01$), and firing rate (ipsilateral movement: Pearson $\rho = 0.05$, Spearman $\rho = 0.13$; contralateral movement: Pearson $\rho = 0.04$, Spearman $\rho = 0.06$) at each movement time point relative to the ITI baseline (Table 4). These data indicate that movement-related changes in β -SPL are independent of both spectral power and firing rate.

DISCUSSION

We sought to understand whether SPL between STN spikes and M1 cortical oscillations in PD subjects, previously reported at rest (Shimamoto et al. 2013), is 1) specific to M1 and 2) modulated during movement. We employed intracranial recording techniques developed by Crowell et al. (2012), while subjects performed a simple motor task, to show that 1) STN-cortex SPL in PD is not specific to M1; 2) SPL is modulated during contralateral movement, independently from changes in oscillatory power; 3) both ipsilateral and contralateral movement is associated with a suppression of SPL, with selective increases in SPL to high-beta oscillations primarily during ipsilateral movement; 4) in a subset of STN neurons, increases in SPL are also associated with both contralateral and ipsilateral movement; and 5) neuronal firing rate responses to movement do not predict movement-related modulation of SPL. These findings demonstrate a potential mechanism through which information transfer occurs in the basal ganglia-thalamocortical loop, involving changes in firing pattern relative to cortical network oscillations.

SPL is not specific to precentral gyrus. Given that the basal ganglia process input from broad cortical regions, we assessed SPL to regions outside of the precentral gyrus. β -SPL to motor cortex has previously been described in PD subjects at rest (Shimamoto et al. 2013). It is important to note, however, that

whereas Shimamoto et al. used a functional designation of primary motor cortex to describe this cortical region, the localization of ECoG electrodes is primarily anatomical. Although the reversal of somatosensory evoked potentials can be used to localize ECoG recordings relative to the central sulcus (Randazzo et al. 2016; Shimamoto et al. 2013), encoding of motor and sensory information is not strictly segregated by this anatomical feature (Desmurget and Sirigu 2015; Huber et al. 2012). Without definitive evidence to dissociate sensory and motor encoding, we preferred to use anatomical designations for electrode placements. Nonetheless, in this work we replicate the results of Shimamoto et al. and further demonstrate that STN neurons phase-lock to broad frontal and parietal cortical areas during periods without movement. Our novel findings that STN neurons participate in SPL with sensory regions is important, because the gating of sensory inputs into other motor areas is one mechanism through which the basal ganglia may participate in motor control (Lidsky et al. 1985; Moore 1987). Indeed, abnormal sensorimotor integration appears to be a key feature in the pathogenesis of many movement disorders (Patel et al. 2014). Given that the STN has also been proposed to play a broad role in the “pausing” of behavior (Aron et al. 2016), it is important to note that although we observed STN neurons that exhibited SPL to premotor cortex, we never observed firing rate modulation before movement onset.

The finding of a negative time lag [median -32 ms, IQR $(-55\ 5)$ ms] associated with the phase synchronization suggests that cortical rhythms may drive STN firing at rest. Shimamoto et al. (2013) also observed a negative time lag, characterized as onset of significant phase-locking (-103 ms), and a peak lag time of -18.5 ms that was not significantly different from zero. Similarly, γ AE-SPL was found across the cortical regions examined, extending the findings of Shimamoto et al. Although the phase lag observed for γ AE-SPL [median -33 ms, IQR $(-174\ 14)$ ms] was similar to that for β -SPL, single neurons exhibiting both types of synchronization often did not lock to the beta and gamma envelope at the same frequency, suggesting that these two modes of oscillatory firing represent distinct network mechanisms that may subserve different aspects of behavior. The γ AE-SPL phase lag was also in agreement with the report of Shimamoto et al. (median onset of 107.1 ms before the spike time, median peak of -48 ms).

We also evaluated whether lag times demonstrated cortical location-specific differences that could be an indirect measure of SPL mechanism. The lag time in our experiments did not significantly differ among neurons phase-locked to different cortical areas. Although we do not have evidence of distinct mechanisms underlying synchronization with different areas of cortex, our sample size among different cortical areas was not great enough to detect subtle differences in lag time. Although the hyperdirect pathway to the STN represents a possible driving influence that could synchronize subthalamic neuronal firing, the primate STN has not been shown to receive direct input from somatosensory

Fig. 7. Examples of STN neuronal phase-locking. *A–C:* example of a neuron whose firing is phase-locked to parietal cortical oscillations at contralateral movement onset. *A:* contralateral (red) and ipsilateral (blue) grip force traces. *B:* β -SPL and γ AE-SPL clusters at each timepoint during contralateral grips. *C:* β -SPL and γ AE-SPL clusters at each timepoint during ipsilateral grips. *D–F:* example of a neuron whose firing is phase-locked to frontal cortical oscillations at ipsilateral movement onset. *D:* contralateral (red) and ipsilateral (blue) grip force traces. *E:* β -SPL and γ AE-SPL clusters at each timepoint during contralateral grips. *F:* β -SPL and γ AE-SPL clusters at each timepoint during ipsilateral grips. Grip force plots show trial-averaged mean (solid or dashed line) and the extrema (shaded region) of the grip force at each time point. Contra, contralateral; Ipsi, ipsilateral.

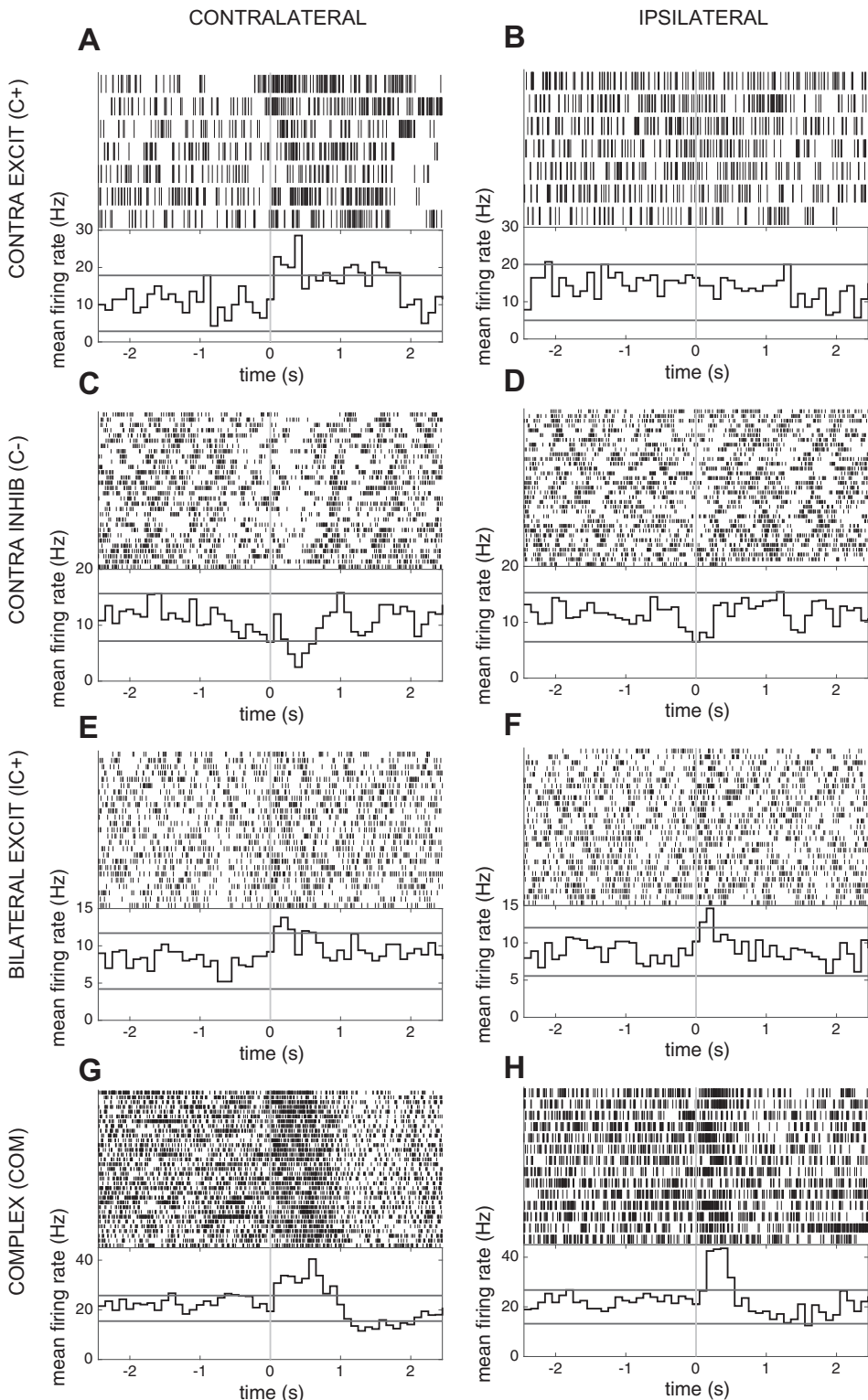


Fig. 8. Examples of task-related unit recordings in the STN during the grip task. Spike rasters (top) and average firing histograms (bottom) aligned on contralateral (*A, C, E, G*) and ipsilateral (*B, D, F, H*) grip force onset show examples of contralateral excitation (*A, B*), contralateral inhibition (*C, D*), bilateral excitation (*E, F*) and complex responses (*G, H*). Red lines in average firing histograms represent the 95% confidence intervals based on the baseline distribution. Excit, excitation; Inhib, inhibition.

cortex, which does project to the striatum (Künzle 1977; Flaherty and Graybiel 1991). Alternatively, the spike-phase synchronization could be maintained via indirect basal ganglia loops.

SPL suppression during contralateral movement occurs independently of oscillatory power changes. Application of grip force with the hand contralateral to recording resulted in a suppression of both β -SPL and γ AE-SPL, on average, in the population of STN neurons recorded. Importantly, changes in

β -SPL relative to ITI baseline were not correlated with the beta power decrease across the movement time course, nor specifically in the 500 ms following movement onset, arguing against the possibility that the SPL data simply reflect the underlying cortical oscillatory power dynamics. It is important to note that the absence of a strong positive correlation does not rule out a relationship between β -SPL and oscillatory power in a subset of the data; however, it shows our ability to measure

Table 4. Changes in β -SPL are independent of spectral power and firing rate during movement

	Pearson ρ	P Value	Spearman ρ	P Value
All time points				
Low- β AW				
Ipsi	0.02	9.42E-02	0.09	2.19E-18
Contra	0.18	0.00E+00	0.17	0.00E+00
High- β AW				
Ipsi	-0.11	2.18E-24	-0.09	1.87E-18
Contra	0.00	8.54E-01	-0.01	2.21E-01
Firing rate				
Ipsi	0.05	3.79E-07	0.13	2.10E-32
Contra	0.04	4.03E-04	0.06	3.90E-08
Movement epoch				
Low- β AW				
Ipsi	0.07	2.48E-02	0.14	1.08E-05
Contra	0.12	1.42E-04	0.16	1.99E-07
High- β AW				
Ipsi	-0.13	4.80E-05	-0.15	2.64E-06
Contra	0.03	3.84E-01	0.01	8.37E-01
Firing rate				
Ipsi	0.09	3.38E-03	0.21	1.14E-11
Contra	-0.07	2.74E-02	-0.01	7.61E-01

Relationships between changes in β -SPL and corresponding changes in low-beta power (Low- β), high-beta power (High- β), and firing rate are summarized at each movement time point (all time points) and the movement epoch (100 to 500 ms following movement onset) relative to the ITI baseline. Oscillatory power is quantified as activation weight (AW). Contra, contralateral; Ipsi, ipsilateral.

SPL independently of oscillatory power. Thus β -SPL suppression appears to represent the uncoupling of STN neural firing from cortical beta rhythms. Although movement is accompanied by marked reductions in these cortical rhythms (Brittain and Brown 2014; Kondylis et al. 2016; Miller et al. 2007), a measurable beta-band oscillation remains in the cortex. In this study, we find a population-level decrease in phase-locking to this remaining beta oscillation.

SPL increase and phase-frequency shift is associated with both contralateral and ipsilateral movement. One of the unique advantages to single-unit recording studies is the insight gained from understanding the heterogeneity of neuronal information encoding. Thus, despite a network-level decrease in β -SPL to cortex within the STN, a distinct subpopulation of STN neurons increased their phase-locking relative to the ITI baseline during contralateral movement. Furthermore, the phase frequency at which neuronal spiking became synchronized within this subpopulation was increased during movement. This frequency shift may represent a mechanism whereby information processing within a specific neuronal functional group is segregated from irrelevant information (Fries 2015). Furthermore, the movement-related frequency shift appears to be driven selectively by frontal and precentral, and not postcentral and parietal, beta oscillations. The apparent functional distinction between low- and high-beta oscillations is not well understood, although the low-beta rhythm has been reported to have greater baseline sensitivity to levodopa than the high-beta rhythm (Foffani et al. 2005; Priori et al. 2004). We previously reported the specificity of robust high-beta movement-related desynchronization in subjects with PD (Kondylis et al. 2016), and it is not known whether the observed phase-frequency shift in this study would occur in subjects without PD.

In addition to SPL modulation by contralateral hand movement, ipsilateral grip force application also resulted in network-level suppression of β -SPL and γ AE-SPL. Similar to contralateral movement, however, a subpopulation of unit-contact pairs showed a significant increase in phase-locking, again suggesting the presence of functionally distinct networks. These ipsilateral movement signals may be mediated via interhemispheric cortico-cortical projections or by cortico-striatal projections (Flaherty and Graybiel 1991). These results again highlight the complex heterogeneity of movement encoding within the STN; however, further work is necessary to fully understand these networks.

Neuronal firing rate responses to movement do not predict movement-related modulation of SPL. Phase-locking during movement was not correlated with movement-related changes in firing rate. SPL during the ITI epoch, as well as movement-related changes in SPL, was independent of the firing-rate movement-related responses of individual STN neurons. This finding is in agreement with Shimamoto et al. (2013), who found no difference in resting SPL between neurons exhibiting responses to arm movement and leg movement as well as nonresponders when examining the proportion of neurons exhibiting M1 beta phase-locking at rest. Our data extend these findings to SPL during movement, indicating that movement-related information transfer can occur in the basal ganglia-subthalamic loop through changes in the pattern of neuronal firing, rather than the total discharge rate. Because no movement-related firing rate changes occurred before movement onset, the decoupling of neuronal firing from beta oscillations that began before movement onset, at a time corresponding to cue presentation, may reflect the cortical response to the cue.

Notably, these findings are based on data collected in patients with PD, and it is not possible to determine the extent to which the dynamics of cortico-subthalamic coupling described reflect normal basal ganglia function vs. a pathological state. Evidence from the 1-methyl-4-phenyl-1,2,3,6-tetrahydropyridine (MPTP) model of PD in nonhuman primates suggests that the disease state involves a loss of selectivity in somatosensory responses, or a broadening of receptive fields, in neurons of the internal segment of the globus pallidus (GPi) (Bergman et al. 1994; Boraud et al. 2000; Leblois et al. 2006). Our finding of STN neuron SPL to oscillatory activity in broadly distributed cortical areas, therefore, may represent a pathological state, with cortico-subthalamic coupling in healthy individuals involving more focal cortical areas. In this study we did not have the statistical power to examine the relationship between the strength of SPL and symptom severity measured as UPDRS motor scores; however, it is important to consider this relationship in future work.

Conclusion. Simultaneous recording of single STN neurons and sensorimotor LFPs in subjects undergoing DBS surgery was used to characterize the dynamics of STN single-neuron phase-locking to beta-band oscillations, and to the amplitude envelope of gamma oscillations, during hand movement. We found that STN SPL is not specific to M1 but is broadly distributed from premotor to sensory cortex. Both β -SPL and γ AE-SPL are suppressed during movement in the population of STN neurons as a whole; however, a subpopulation of STN neurons becomes selectively phase-locked during movement. These dynamic and heterogeneous interactions occurred independently of event-related changes in STN firing rates and

cortical beta-band power, highlighting limitations of existing firing rate-based models of basal ganglia function. Thus our findings demonstrate the encoding of movement by networks of STN neurons via dynamic phase synchronization with pre-motor, motor, and sensory cortices, but further work is needed to understand the role of these interactions in normal and PD-associated basal ganglia function.

ACKNOWLEDGMENTS

We thank Jonathan Rubin for comments on the manuscript and Jim Sweat and Matt Bartosiewicz for expert assistance in the operating room.

GRANTS

R. M. Richardson was supported in part by the Walter L. Copeland Fund of The Pittsburgh Foundation. W. J. Lipski was supported by National Institute of Mental Health Grant R01MH107797 (PI, Avniel Ghuman; co-investigator, R. M. Richardson).

DISCLOSURES

No conflicts of interest, financial or otherwise, are declared by the authors.

AUTHOR CONTRIBUTIONS

W.J.L., R.S.T., D.J.C., and R.M.R. conceived and designed research; W.J.L., T.A.W., A.A., D.J.C., and R.M.R. performed experiments; W.J.L., T.A.W., A.A., and E.K. analyzed data; W.J.L., T.A.W., A.A., E.K., R.S.T., D.J.C., and R.M.R. interpreted results of experiments; W.J.L. prepared figures; W.J.L. drafted manuscript; W.J.L., T.A.W., A.A., E.K., R.S.T., D.J.C., and R.M.R. edited and revised manuscript; W.J.L., T.A.W., A.A., E.K., R.S.T., D.J.C., and R.M.R. approved final version of manuscript.

REFERENCES

- Abosch A, Hutchison WD, Saint-Cyr JA, Dostrovsky JO, Lozano AM.** Movement-related neurons of the subthalamic nucleus in patients with Parkinson disease. *J Neurosurg* 97: 1167–1172, 2002. doi:[10.3171/jns.2002.97.5.1167](https://doi.org/10.3171/jns.2002.97.5.1167).
- Afsharpour S.** Topographical projections of the cerebral cortex to the subthalamic nucleus. *J Comp Neurol* 236: 14–28, 1985. doi:[10.1002/cne.902360103](https://doi.org/10.1002/cne.902360103).
- Alegre M, Lopez-Azcarate J, Obeso I, Wilkinson L, Rodriguez-Oroz MC, Valencia M, Garcia-Garcia D, Guridi J, Artieda J, Jahanshahi M, Obeso JA.** The subthalamic nucleus is involved in successful inhibition in the stop-signal task: a local field potential study in Parkinson's disease. *Exp Neurol* 239: 1–12, 2013. doi:[10.1016/j.expneurol.2012.08.027](https://doi.org/10.1016/j.expneurol.2012.08.027).
- Aron AR, Herz DM, Brown P, Forstmann BU, Zaghloul K.** Frontosubthalamic circuits for control of action and cognition. *J Neurosci* 36: 11489–11495, 2016. doi:[10.1523/JNEUROSCI.2348-16.2016](https://doi.org/10.1523/JNEUROSCI.2348-16.2016).
- Bergman H, Wichmann T, Karmon B, DeLong MR.** The primate subthalamic nucleus. II. Neuronal activity in the MPTP model of parkinsonism. *J Neurophysiol* 72: 507–520, 1994.
- Bevan MD, Magill PJ, Terman D, Bolam JP, Wilson CJ.** Move to the rhythm: oscillations in the subthalamic nucleus-external globus pallidus network. *Trends Neurosci* 25: 525–531, 2002. doi:[10.1016/S0166-2236\(02\)02235-X](https://doi.org/10.1016/S0166-2236(02)02235-X).
- Boraud T, Bezard E, Bioulac B, Gross CE.** Ratio of inhibited-to-activated pallidal neurons decreases dramatically during passive limb movement in the MPTP-treated monkey. *J Neurophysiol* 83: 1760–1763, 2000.
- Brittain JS, Brown P.** Oscillations and the basal ganglia: motor control and beyond. *Neuroimage* 85: 637–647, 2014. doi:[10.1016/j.neuroimage.2013.05.084](https://doi.org/10.1016/j.neuroimage.2013.05.084).
- Brown P.** Oscillatory nature of human basal ganglia activity: relationship to the pathophysiology of Parkinson's disease. *Mov Disord* 18: 357–363, 2003. doi:[10.1002/mds.10358](https://doi.org/10.1002/mds.10358).
- Canteras NS, Shammah-Lagnado SJ, Silva BA, Ricardo JA.** Afferent connections of the subthalamic nucleus: a combined retrograde and anterograde horseradish peroxidase study in the rat. *Brain Res* 513: 43–59, 1990. doi:[10.1016/0006-8993\(90\)91087-W](https://doi.org/10.1016/0006-8993(90)91087-W).
- Crowell AL, Ryapolova-Webb ES, Ostrem JL, Galifianakis NB, Shimamoto S, Lim DA, Starr PA.** Oscillations in sensorimotor cortex in movement disorders: an electrocorticography study. *Brain* 135: 615–630, 2012. doi:[10.1093/brain/awr332](https://doi.org/10.1093/brain/awr332).
- Dale AM, Fischl B, Sereno MI.** Cortical surface-based analysis. I. Segmentation and surface reconstruction. *Neuroimage* 9: 179–194, 1999. doi:[10.1006/nimg.1998.0395](https://doi.org/10.1006/nimg.1998.0395).
- DeLong MR, Crutcher MD, Georgopoulos AP.** Primate globus pallidus and subthalamic nucleus: functional organization. *J Neurophysiol* 53: 530–543, 1985.
- DeLong MR, Wichmann T.** Circuits and circuit disorders of the basal ganglia. *Arch Neurol* 64: 20–24, 2007. doi:[10.1001/archneur.64.1.20](https://doi.org/10.1001/archneur.64.1.20).
- Delorme A, Makeig S.** EEGLAB: an open source toolbox for analysis of single-trial EEG dynamics including independent component analysis. *J Neurosci Methods* 134: 9–21, 2004. doi:[10.1016/j.jneumeth.2003.10.009](https://doi.org/10.1016/j.jneumeth.2003.10.009).
- Desikan RS, Ségonne F, Fischl B, Quinn BT, Dickerson BC, Blacker D, Buckner RL, Dale AM, Maguire RP, Hyman BT, Albert MS, Killiany RJ.** An automated labeling system for subdividing the human cerebral cortex on MRI scans into gyral based regions of interest. *Neuroimage* 31: 968–980, 2006. doi:[10.1016/j.neuroimage.2006.01.021](https://doi.org/10.1016/j.neuroimage.2006.01.021).
- Desmurget M, Sirigu A.** Revealing humans' sensorimotor functions with electrical cortical stimulation. *Philos Trans R Soc Lond B Biol Sci* 370: 20140207, 2015. doi:[10.1098/rstb.2014.0207](https://doi.org/10.1098/rstb.2014.0207).
- Flaherty AW, Graybiel AM.** Corticostriatal transformations in the primate somatosensory system. Projections from physiologically mapped body-part representations. *J Neurophysiol* 66: 1249–1263, 1991.
- Foffani G, Bianchi AM, Baselli G, Priori A.** Movement-related frequency modulation of beta oscillatory activity in the human subthalamic nucleus. *J Physiol* 568: 699–711, 2005. doi:[10.1113/jphysiol.2005.089722](https://doi.org/10.1113/jphysiol.2005.089722).
- Fries P.** Rhythms for cognition: communication through coherence. *Neuron* 88: 220–235, 2015. doi:[10.1016/j.neuron.2015.09.034](https://doi.org/10.1016/j.neuron.2015.09.034).
- Gale JT, Shields DC, Jain FA, Amirnovin R, Eskandar EN.** Subthalamic nucleus discharge patterns during movement in the normal monkey and Parkinsonian patient. *Brain Res* 1260: 15–23, 2009. doi:[10.1016/j.brainres.2008.12.062](https://doi.org/10.1016/j.brainres.2008.12.062).
- Georgopoulos AP, DeLong MR, Crutcher MD.** Relations between parameters of step-tracking movements and single cell discharge in the globus pallidus and subthalamic nucleus of the behaving monkey. *J Neurosci* 3: 1586–1598, 1983.
- Hammond C, Bergman H, Brown P.** Pathological synchronization in Parkinson's disease: networks, models and treatments. *Trends Neurosci* 30: 357–364, 2007. doi:[10.1016/j.tins.2007.05.004](https://doi.org/10.1016/j.tins.2007.05.004).
- Haynes WI, Haber SN.** The organization of prefrontal-subthalamic inputs in primates provides an anatomical substrate for both functional specificity and integration: implications for Basal Ganglia models and deep brain stimulation. *J Neurosci* 33: 4804–4814, 2013. doi:[10.1523/JNEUROSCI.4674-12.2013](https://doi.org/10.1523/JNEUROSCI.4674-12.2013).
- Huber D, Gutnisky DA, Peron S, O'Connor DH, Wieger JS, Tian L, Oertner TG, Looger LL, Svoboda K.** Multiple dynamic representations in the motor cortex during sensorimotor learning. *Nature* 484: 473–478, 2012. doi:[10.1038/nature11039](https://doi.org/10.1038/nature11039).
- Kondylis ED, Randazzo MJ, Alhourani A, Lipski WJ, Wozny TA, Pandya Y, Ghuman AS, Turner RS, Crammond DJ, Richardson RM.** Movement-related dynamics of cortical oscillations in Parkinson's disease and essential tremor. *Brain* 139: 2211–2223, 2016. doi:[10.1093/brain/aww144](https://doi.org/10.1093/brain/aww144).
- Kühn AA, Tsui A, Aziz T, Ray N, Brücke C, Kupsch A, Schneider G-H, Brown P.** Pathological synchronisation in the subthalamic nucleus of patients with Parkinson's disease relates to both bradykinesia and rigidity. *Exp Neurol* 215: 380–387, 2009. doi:[10.1016/j.expneurol.2008.11.008](https://doi.org/10.1016/j.expneurol.2008.11.008).
- Künzle H.** Projections from the primary somatosensory cortex to basal ganglia and thalamus in the monkey. *Exp Brain Res* 30: 481–492, 1977. doi:[10.1007/BF00237639](https://doi.org/10.1007/BF00237639).
- Leblois A, Meissner W, Bezard E, Bioulac B, Gross CE, Boraud T.** Temporal and spatial alterations in GPi neuronal encoding might contribute to slow down movement in Parkinsonian monkeys. *Eur J Neurosci* 24: 1201–1208, 2006. doi:[10.1111/j.1460-9568.2006.04984.x](https://doi.org/10.1111/j.1460-9568.2006.04984.x).
- Lidsky TI, Manetto C, Schneider JS.** A consideration of sensory factors involved in motor functions of the basal ganglia. *Brain Res* 9: 133–146, 1985. doi:[10.1016/0165-0173\(85\)90010-4](https://doi.org/10.1016/0165-0173(85)90010-4).
- Maris E, Oostenveld R.** Nonparametric statistical testing of EEG- and MEG-data. *J Neurosci Methods* 164: 177–190, 2007. doi:[10.1016/j.jneumeth.2007.03.024](https://doi.org/10.1016/j.jneumeth.2007.03.024).
- Miller KJ, Leuthardt EC, Schalk G, Rao RPN, Anderson NR, Moran DW, Miller JW, Ojemann JG.** Spectral changes in cortical surface potentials

- during motor movement. *J Neurosci* 27: 2424–2432, 2007. doi:[10.1523/JNEUROSCI.3886-06.2007](https://doi.org/10.1523/JNEUROSCI.3886-06.2007).
- Moore AP.** Impaired sensorimotor integration in parkinsonism and dyskinesia: a role for corollary discharges? *J Neurol Neurosurg Psychiatry* 50: 544–552, 1987. doi:[10.1136/jnnp.50.5.544](https://doi.org/10.1136/jnnp.50.5.544).
- Nambu A, Tokuno H, Inase M, Takada M.** Corticosubthalamic input zones from forelimb representations of the dorsal and ventral divisions of the premotor cortex in the macaque monkey: comparison with the input zones from the primary motor cortex and the supplementary motor area. *Neurosci Lett* 239: 13–16, 1997. doi:[10.1016/S0304-3940\(97\)00877-X](https://doi.org/10.1016/S0304-3940(97)00877-X).
- Parent A, Hazrati LN.** Functional anatomy of the basal ganglia. II. The place of subthalamic nucleus and external pallidum in basal ganglia circuitry. *Brain Res Brain Res Rev* 20: 128–154, 1995. doi:[10.1016/0165-0173\(94\)0008-D](https://doi.org/10.1016/0165-0173(94)0008-D).
- Patel N, Jankovic J, Hallett M.** Sensory aspects of movement disorders. *Lancet Neurol* 13: 100–112, 2014. doi:[10.1016/S1474-4422\(13\)70213-8](https://doi.org/10.1016/S1474-4422(13)70213-8).
- Priori A, Foffani G, Pesenti A, Tamia F, Bianchi AM, Pellegrini M, Locatelli M, Moxon KA, Villani RM.** Rhythm-specific pharmacological modulation of subthalamic activity in Parkinson's disease. *Exp Neurol* 189: 369–379, 2004. doi:[10.1016/j.expneurol.2004.06.001](https://doi.org/10.1016/j.expneurol.2004.06.001).
- Randazzo MJ, Kondylis ED, Alhourani A, Wozny TA, Lipski WJ, Crammond DJ, Richardson RM.** Three-dimensional localization of cortical electrodes in deep brain stimulation surgery from intraoperative fluoroscopy. *Neuroimage* 125: 515–521, 2016. doi:[10.1016/j.neuroimage.2015.10.076](https://doi.org/10.1016/j.neuroimage.2015.10.076).
- Rivlin-Etzion M, Ritov Y, Heimer G, Bergman H, Bar-Gad I.** Local shuffling of spike trains boosts the accuracy of spike train spectral analysis. *J Neurophysiol* 95: 3245–3256, 2006. doi:[10.1152/jn.00055.2005](https://doi.org/10.1152/jn.00055.2005).
- Rodriguez-Oroz MC, Rodriguez M, Guridi J, Mewes K, Chockman V, Vitek J, DeLong MR, Obeso JA.** The subthalamic nucleus in Parkinson's disease: somatotopic organization and physiological characteristics. *Brain* 124: 1777–1790, 2001. doi:[10.1093/brain/124.9.1777](https://doi.org/10.1093/brain/124.9.1777).
- Romanelli P, Heit G, Hill BC, Kraus A, Hastie T, Brontë-Stewart HM.** Microelectrode recording revealing a somatotopic body map in the subthalamic nucleus in humans with Parkinson disease. *J Neurosurg* 100: 611–618, 2004. doi:[10.3171/jns.2004.100.4.0611](https://doi.org/10.3171/jns.2004.100.4.0611).
- Schrock LE, Ostrem JL, Turner RS, Shimamoto SA, Starr PA.** The subthalamic nucleus in primary dystonia: single-unit discharge characteristics. *J Neurophysiol* 102: 3740–3752, 2009. doi:[10.1152/jn.00544.2009](https://doi.org/10.1152/jn.00544.2009).
- Shimamoto SA, Ryapolova-Webb ES, Ostrem JL, Galifianakis NB, Miller KJ, Starr PA.** Subthalamic nucleus neurons are synchronized to primary motor cortex local field potentials in Parkinson's disease. *J Neurosci* 33: 7220–7233, 2013. doi:[10.1523/JNEUROSCI.4676-12.2013](https://doi.org/10.1523/JNEUROSCI.4676-12.2013).
- Starr PA, Theodosopoulos PV, Turner R.** Surgery of the subthalamic nucleus: use of movement-related neuronal activity for surgical navigation. *Neurosurgery* 53: 1146–1149, 2003. doi:[10.1227/01.NEU.0000088803.79153.05](https://doi.org/10.1227/01.NEU.0000088803.79153.05).
- Stebbins GT, Goetz CG, Burn DJ, Jankovic J, Khoo TK, Tilley BC.** How to identify tremor dominant and postural instability/gait difficulty groups with the movement disorder society unified Parkinson's disease rating scale: comparison with the unified Parkinson's disease rating scale. *Mov Disord* 28: 668–670, 2013. doi:[10.1002/mds.25383](https://doi.org/10.1002/mds.25383).
- Steigerwald F, Pötter M, Herzog J, Pinsker M, Kopper F, Mehndorn H, Deuschl G, Volkmann J.** Neuronal activity of the human subthalamic nucleus in the parkinsonian and nonparkinsonian state. *J Neurophysiol* 100: 2515–2524, 2008. doi:[10.1152/jn.90574.2008](https://doi.org/10.1152/jn.90574.2008).
- Theodosopoulos PV, Marks WJ Jr, Christine C, Starr PA.** Locations of movement-related cells in the human subthalamic nucleus in Parkinson's disease. *Mov Disord* 18: 791–798, 2003. doi:[10.1002/mds.10446](https://doi.org/10.1002/mds.10446).
- Turner RS, Desmurget M.** Basal ganglia contributions to motor control: a vigorous tutor. *Curr Opin Neurobiol* 20: 704–716, 2010. doi:[10.1016/j.conb.2010.08.022](https://doi.org/10.1016/j.conb.2010.08.022).
- Wichmann T, Bergman H, DeLong MR.** The primate subthalamic nucleus. I. Functional properties in intact animals. *J Neurophysiol* 72: 494–506, 1994.
- Yang AI, Vanegas N, Lungu C, Zaghloul KA.** Beta-coupled high-frequency activity and beta-locked neuronal spiking in the subthalamic nucleus of Parkinson's disease. *J Neurosci* 34: 12816–12827, 2014. doi:[10.1523/JNEUROSCI.1895-14.2014](https://doi.org/10.1523/JNEUROSCI.1895-14.2014).
- Zaghloul KA, Weidemann CT, Lega BC, Jaggi JL, Baltuch GH, Kahana MJ.** Neuronal activity in the human subthalamic nucleus encodes decision conflict during action selection. *J Neurosci* 32: 2453–2460, 2012. doi:[10.1523/JNEUROSCI.5815-11.2012](https://doi.org/10.1523/JNEUROSCI.5815-11.2012).
- Zavala B, Damera S, Dong JW, Lungu C, Brown P, Zaghloul KA.** Human subthalamic nucleus theta and beta oscillations entrain neuronal firing during sensorimotor conflict. *Cereb Cortex* 27: 496–508, 2017. doi:[10.1093/cercor/bhw244](https://doi.org/10.1093/cercor/bhw244).
- Zavala B, Tan H, Ashkan K, Foltyne T, Limousin P, Zrinzo L, Zaghloul K, Brown P.** Human subthalamic nucleus-medial frontal cortex theta phase coherence is involved in conflict and error related cortical monitoring. *Neuroimage* 137: 178–187, 2016. doi:[10.1016/j.neuroimage.2016.05.031](https://doi.org/10.1016/j.neuroimage.2016.05.031).
- Zavala BA, Tan H, Little S, Ashkan K, Hariz M, Foltyne T, Zrinzo L, Zaghloul KA, Brown P.** Midline frontal cortex low-frequency activity drives subthalamic nucleus oscillations during conflict. *J Neurosci* 34: 7322–7333, 2014. doi:[10.1523/JNEUROSCI.1169-14.2014](https://doi.org/10.1523/JNEUROSCI.1169-14.2014).